Chemistry & Biology
Article

Deconvolution of the Cellular Oxidative Stress Response with Organelle-Specific Peptide Conjugates

Kerry P. Mahon,[1,5] Terra B. Potocky,[1,2,5] Derek Blair,[2] Marc D. Roy,[1] Kelly M. Stewart,[3] Thomas C. Chiles,[2] and Shana O. Kelley[1,3,4,*]
[1]Department of Chemistry
[2]Department of Biology
Boston College, Chestnut Hill, MA 02467, USA
[3]Department of Biochemistry
[4]Department of Pharmaceutical Sciences
Leslie Dan Faculty of Pharmacy, University of Toronto, Toronto, Ontario M5S 3M2, Canada
[5]These authors contributed equally to this work.
*Correspondence: shana.kelley@utoronto.ca
DOI 10.1016/j.chembiol.2007.07.011

SUMMARY

Oxidative stress is a deleterious force that must be combated relentlessly by aerobic organisms and is known to underlie many human diseases including atherosclerosis, Parkinson's disease, and Alzheimer's disease. Information available about the oxidative stress response has come primarily from studies using reactive oxygen species (ROS) with ill-defined locations within the cell. Thus, existing models do not account for possible differences between stress originating within particular regions of the cell. Here, oxidative stress is studied at the subcellular level using ROS-generating compounds localizing within two different organelles: the nucleus and the mitochondrion. Differences in cytotoxicity, gene expression, and survival pathway activation are detected as a function of the subcellular origin of oxidative stress, indicating that independent mechanisms are used to cope with oxidative stress arising in different cellular compartments. These comparative studies, enabled by the development of organelle-specific oxidants, examine the cellular responses to site-specific oxidative stress with heightened precision.

INTRODUCTION

Oxidative stress severely impacts cellular function by damaging important cellular components. The presence of oxidized DNA, protein, and lipids is correlated with a variety of disease states and the aging process [1, 2], indicating that the disruption in cellular function caused by oxidative damage also interferes with physiological function. Biological systems have many lines of defense against this type of stress, including repair enzymes and targeted degradation pathways that can combat low levels of damage and allow cellular function to proceed [2–6]. Other defense pathways, however, can signal that apoptotic cell death is required under conditions of severe stress [7].

Although prior studies of oxidative stress have elucidated important pathways representing the cellular response to this insult [3, 5], there is little information linking the subcellular origin of oxidative stress with the eventual outcome. In particular, although oxidative damage is known to occur in both the nuclei and mitochondria of living cells [4, 8], it is not known how the cellular response differs when stress originates in these separate compartments. Although endogenous oxidative stress caused by byproducts of oxidative phosphorylation is unavoidable in the mitochondria of living cells, it is exogenous agents or side reactions resulting from redox signaling that may produce stress in the nuclei of cells. It is therefore likely that different mechanisms are used to cope with distinct types of oxidative stress. Nonetheless, most studies of this phenomenon rely on reactive species that are not confined to a given area of the cell (e.g., H_2O_2), and thus results obtained include contributions from stress arising in different cellular compartments.

If studying oxidative stress at the subcellular level were made possible, a number of provocative questions could be posed. Are reactive oxygen species (ROS) generated in different organelles equally toxic? If ROS-triggered cell death occurs, does it proceed via the same mechanism if the oxidants are generated in different compartments? And, does the cell use the same defenses or generate the same responses to oxidative stress initiated at different sites? The opportunity to answer these questions would yield insights into the level of specificity inherent in the defenses that cells use to combat oxidative stress.

To probe site-specific stress within living cells, we have developed a class of compounds that can be used to generate oxidative stress within individual organelles. Using these delivery agents, we have studied how nuclear and mitochondrial stress affect cellular viability, determined

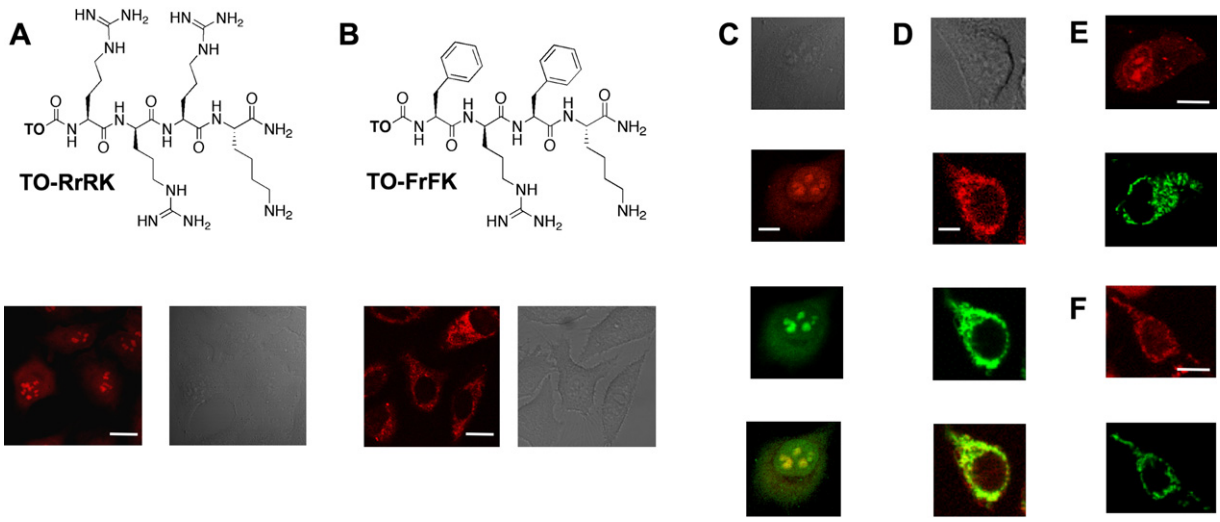

Figure 1. Structures and Localization Profiles for Peptidoconjugate Oxidants

(A) Structure and fluorescence confocal microscopy images for TO-RrRK demonstrating localization of this compound within the nuclei of living, unfixed HeLa cells. Images were acquired after incubating cells with 5 μM conjugate for 1.5 hr. Fluorescence image (left) is shown alongside corresponding DIC image (right). The scale bar represents 10 μm.

(B) Structure and fluorescence confocal microscopy images for TO-FrFK demonstrating localization of this compound within the mitochondria of living, unfixed HeLa cells. Fluorescence image (left) is shown alongside corresponding DIC image (right). The scale bar represents 10 μm. The conditions listed above also apply to this experiment. Illumination conditions were optimized such that cell viability and integrity were maintained, with laser power confined to levels where no toxicity would be observed. The localization patterns were highly reproducible and were observed in >20 separate trials (see the Supplemental Data for additional images).

(C) Colocalization of TO-RrRK (red) with Syto 60 (green). Quantitation of nuclear overlap using the CoLocalizer Pro software package produced a Pearson's coefficient of +0.69 ± 0.04. The scale bar represents 5 μm.

(D) Colocalization of TO-FrFK (red) with deep red mitotracker 633 (green). Quantitation of overlap using the CoLocalizer Pro software package produced a Pearson's coefficient of +0.77 ± 0.09. The scale bar represents 5 μm.

(E) Colocalization of TO-RrRK (red) with mitotracker (green) in MRC-5 cells.

(F) Colocalization of TO-FrFK (red) with mitotracker (green) in MRC-5 cells. See the Supplemental Data for additional experimental data concerning localization of the conjugates.

that the mechanism of death involves apoptosis and is independent of the origin of oxidative stress, and evaluated the signaling pathways and the genome-wide response provoked by mitochondrial and nuclear oxidative stress. The results indicate that cellular pathways are utilized in patterns specific to each type of stress.

RESULTS AND DISCUSSION

Two peptidoconjugates with specific cellular localization profiles were developed to separately address oxidative stress occurring in the nuclei and mitochondria of living HeLa cells (Figure 1). These conjugates feature thiazole orange (TO), a chromophore that produces singlet oxygen ($^1O_2$) upon exposure to visible light [9, 10]. TO is also highly fluorescent in viscous or rigid media and provides a means to image the conjugates within cells to determine spatial localization [11]. Two peptide sequences were developed that impart different organellar localizations to the conjugates: FrFK (r = *d*-arginine) and RrRK. As shown in images obtained by confocal fluorescence microscopy (Figure 1), TO-RrRK appears primarily in the nuclei of live cells (Figure 1A), whereas TO-FrFK localizes primarily within mitochondria (Figure 1B). Both localization profiles were confirmed in colocalization experiments as shown in Figures 1C and 1D. The origin of the distinct localization profiles observed for these compounds may result from the different molecular charges of TO-FrFK and TO-RrRK. Lipophilic cations typically localize to mitochondria, but an excess of molecular charge can prevent a peptide from accessing this organelle because of the hydrophobicity of the mitochondrial inner membrane [12]. Hence, it is more favorable for TO-FrFK, bearing a +3 charge, to achieve mitochondrial localization than TO-RrRK, which possesses a +5 charge. It is noteworthy that both compounds cross the plasma membrane with efficiencies that approach what has been previously observed for the longer Tat peptide [13] (K.L. Horton, K.M.S., K.P.M., J. Rose, and S.O.K., unpublished data). The positive charges of the compounds, and the use of a positively charged chromophore, enable efficient uptake of these smaller conjugates.

To use organelle-specific peptide conjugates to generate oxidative stress within nuclei and mitochondria, cells containing either TO-FrFK or TO-RrRK were exposed to visible light of 501 nm. When the compounds were tested in vitro, similar levels of biomolecular damage were observed, indicating that the two agents could generate

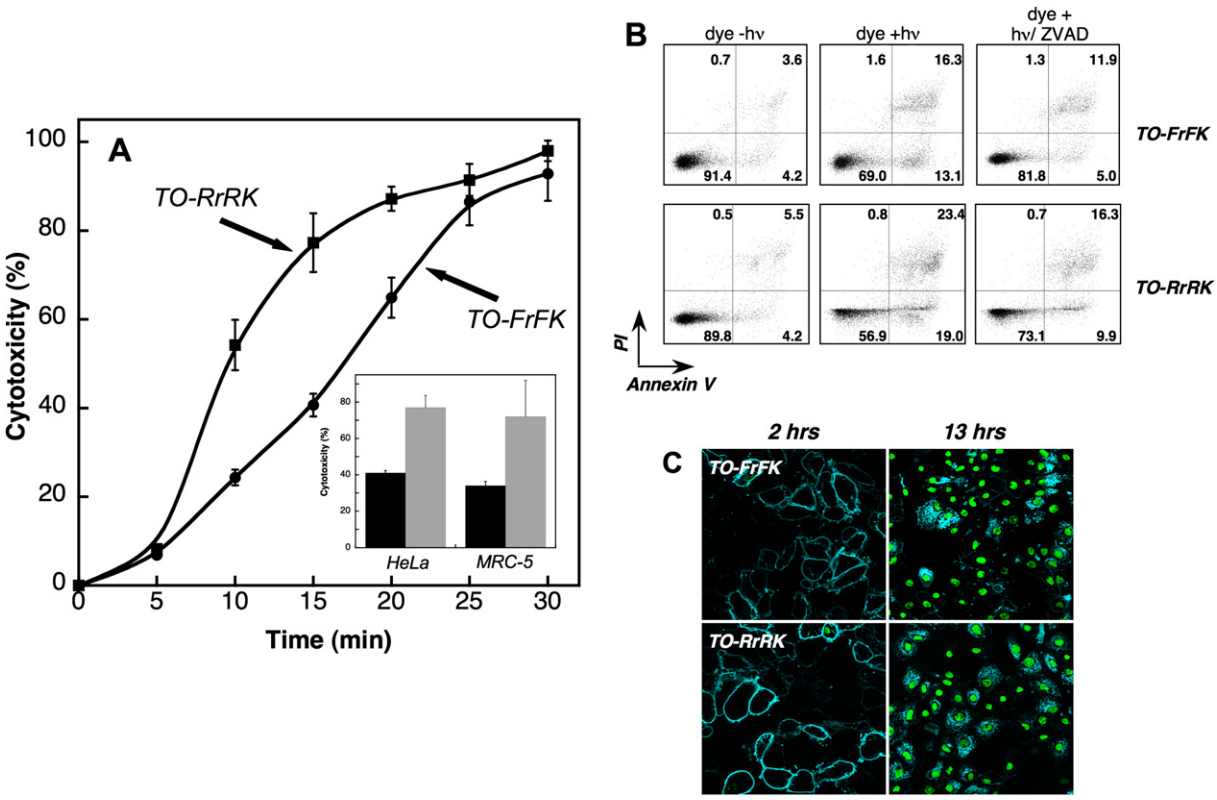

Figure 2. Toxicity and Mechanism of Cell Death Characterizing Nuclear and Mitochondrial Oxidative Stress

(A) Measurement of cytotoxicity using the CCK-8 assay for HeLa cells subjected to incubation with either 5 μM TO-FrFK or TO-RrRK followed by irradiation for 0–30 min. Cells were allowed to recover for 13 hr after irradiation, and then incubated with CCK-8 dye for 2 hr. The amount of NADPH reduction of CCK-8 was measured at 450 nm. Cells were not affected by the presence of TO-FrFK or TO-RrRK alone, or light exposure alone. Error shown represents standard error. Inset: comparison of the phototoxicity of TO-RrRK (gray) and TO-FrFK (black) in HeLa and MRC-5 cells. Samples were irradiated for 15 min and then incubated and analyzed as above.

(B) Measurement of apoptotic cell death caused by ROS generated by TO-RrRK and TO-FrFK by flow cytometry. Treated cells were incubated with Cy5-Annexin V and propidium iodide (PI) and analyzed by flow cytometry. Values shown in each quadrant correspond to percentages of cells observed in one experimental trial; results consistent with these were obtained in three independent trials. To assess the effect of an apoptosis inhibitor, cells were incubated with 50 μM zVAD-FMK during treatment and recovery.

(C) Analysis of mechanism of cell death using confocal microscopy. Two hours after irradiation (left), cells were treated with Cy5-Annexin V and PI and imaged. The absence of PI staining along with Annexin V staining of the plasma membrane at 2 hr is consistent with apoptotic, rather than necrotic, cell death. At 13 hr (right), compromised membranes and condensed nuclei are observed, again consistent with apoptosis.

comparable levels of ROS (see the Supplemental Data available with this article online). In living cells, whereas the viabilities of cells that were exposed to conjugate alone or light alone were not affected, significant levels of cell death were observed when oxidative stress was initiated via the excitation of either TO-FrFK or TO-RrRK (Figure 2A). Interestingly, the compound localized to the nucleus, TO-RrRK, caused significantly higher levels of cell death than the mitochondrially localized TO-FrFK. This result was confirmed in the human lung fibroblast cell line MRC-5, where the organelle-specific oxidants also display differential localization (Figures 1E and 1F). When MRC-5 cells were subjected to stress induced by either TO-FrFK or TO-RrRK, the same trend in toxicity levels was observed (Figure 2A). Although these results suggest that nuclear oxidative stress is more toxic than mitochondrial oxidative stress, the exact levels of ROS generated in different compartments of living cells—which cannot be determined in this experimental system—could influence the toxicity levels observed.

The mechanism of cell death promoted by oxidative stress triggered in either the nuclei or mitochondria of living cells was probed using flow cytometry (Figure 2B). When flow cytometry was performed in conjunction with Cy5-Annexin V/propidium iodide (PI) staining for the identification of apoptotic and necrotic cells, apoptotic cells were observed in samples treated with both compounds. The treatment of cells with the antiapoptotic factor zVAD (a general caspase inhibitor) caused a decrease in the number of cells identified by flow cytometry as apoptotic, validating the assignment of this population.

Confocal fluorescence microscopy was also employed to visualize morphological changes brought on by oxidative stress. As shown in Figure 2C, surface-bound Annexin

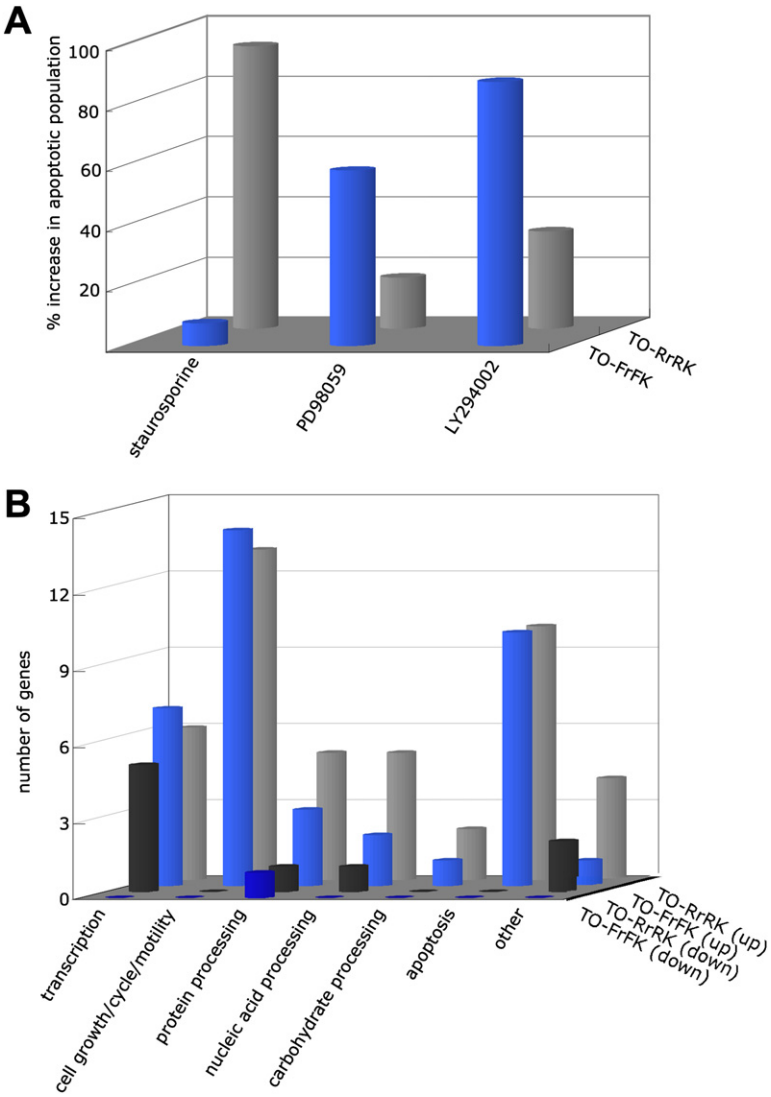

Figure 3. Deconvolution of Mitochondrial and Nuclear Stress by Analysis of Survival Pathway Inhibition and Genome-Wide Gene Expression Profiling

(A) Effects of inhibition of three different survival pathways on TO-FrFK- and TO-RrRK-induced apoptosis. TO-FrFK- and TO-RrRK-irradiated cells were incubated for 15 hr in the presence of staurosporine (5 nM), PD98059 (25 μM), or LY294002 (10 μM). Concentrations of inhibitors used were not toxic alone. Treated cells were incubated with Cy5-Annexin V and propidium iodide (PI) and analyzed by flow cytometry. The percentage of apoptotic cells was calculated as the sum of Annexin V-positive and Annexin V/PI double-positive cells, which accurately reflects levels of late-stage apoptotic cells. See Figure S3 for raw data used to determine changes in apoptotic levels and error levels. Results were obtained from the averages of at least three individual experiments.

(B) Gene expression analysis for mitochondrial and nuclear oxidative stress. A genome-wide profiling experiment, performed with a human Affymetrix chip covering 47,000 genes, was performed with RNA isolated from cells irradiated in the presence of TO-RrRK or TO-FrFK. Differentially expressed genes were identified by comparing gene expression levels of irradiated to nonirradiated samples and grouped into categories. The genes identified from this analysis were grouped into categories according to the functions shown on the x axis. The number of genes in each category is shown for each conjugate and quantitated on the y axis. Genes shown in the first two rows were downregulated (TO-FrFK down, dark blue; TO-RrRK down, black), whereas genes shown in the second two rows were upregulated (TO-FrFK up, light blue; TO-RrRK up, gray). The experiment was performed in triplicate. The identities of all genes identified can be found in Supplemental Data.

V was observed 2 hr after irradiation, whereas no PI staining was observed in cells treated with both compounds. These observations are consistent with apoptosis as the mechanism of cell death, given that the cell membrane should be impermeable in early-stage apoptosis. At later times (e.g., 13 hr), Annexin V and PI could be visualized inside the cell, and condensed nuclei were apparent. In late-stage apoptosis, the cell membrane is compromised, and PI and Annexin V can enter the cell. These results, taken together, indicate that apoptosis is the primary pathway for cell death resulting from oxidative stress initiated either in the nuclei or mitochondria of HeLa cells.

In order to determine whether apoptosis-related signal transduction cascades were differentially affected by mitochondrial or nuclear oxidative stress, we tested the effects of a series of inhibitors that are known to block survival pathways that suppress apoptosis (Figure 3A). The activation of different survival pathways in response to organelle-specific oxidative stress was evaluated using cell-permeable molecules that specifically inhibit the PKC, MAPK/ERK, and PI3K survival pathways: staurosporine [14], PD98059 [15], and LY294002 [16], respectively. Cells were incubated with TO-peptide conjugate, irradiated, and inhibitor was added immediately after irradiation. Levels of apoptosis compared to controls were then quantitated using flow cytometry. Staurosporine, an inhibitor of PKC signaling, induced large increases in apoptosis levels for TO-RrRK-treated cells, but had no appreciable effect on cells treated with TO-FrFK. In contrast, treatment with PD98059, an inhibitor of ERK signaling, resulted in significantly increased apoptosis in TO-FrFK-treated cells, but had a small effect on TO-RrRK-induced apoptosis. Therefore, ERK signaling seems to be more heavily involved in the survival response to mitochondrial oxidative stress, whereas the PKC survival pathway appears to be more specifically involved in cellular protection from nuclear oxidative stress. In addition, inhibition of the PI3K survival pathway by LY294002 resulted

Table 1. Gene Expression Changes Measured by Real-Time PCR for Mitochondrial (TO-FrFK) and Nuclear (TO-RrRK) Oxidative Stress in HeLa Cells

Gene	Fold Change	
	TO-FrFK	TO-RrRK
TO-FrFK > TO-RrRK		
areg	4.8 (0.8)	2.8 (0.5)
ereg	3.0 (1.0)	0.8 (0.2)
egr3	38 (4)	6 (1)
TO-FrFK = TO-RrRK		
cox2	11 (1)	8 (2)
btg2	6 (2)	8 (1)
gadd45b	5 (1)	7 (1)
TO-FrFK < TO-RrRK		
atf3	18 (3)	48 (1)
jun	9 (3)	22 (7)

areg, amphiregulin; *ereg*, epiregulin; *egr3*, early growth response 3; *cox2*, cyclooxygenase-2; *btg2*, BTG family, member 2; *gadd45b*, growth arrest and DNA damage inducible, β; *atf3*, activating transcription factor 3; *jun*, v-jun avian sarcoma virus 17 oncogene. Numbers in parentheses represent standard deviation values.

in increased apoptosis upon treatment with either TO-FrFK or TO-RrRK, indicating that this pathway may be activated upon both nuclear and mitochondrial oxidative stress. However, the inhibition of this pathway has a much larger effect on levels of apoptosis in cells subjected to mitochondrial oxidative stress. These results suggest that different combinations of survival pathways may be activated depending on the origin of the oxidative stress in the cell.

Genome-wide screens of oxidative stress in mammalian cells have allowed for the identification of a distinct set of genes affected by this type of insult [5]. However, the subset of genes regulated by oxidative stress occurring in specific subcellular organelles remains unidentified. To further elucidate the cellular response to oxidative stress originating in mitochondria or nuclei, a genome-wide expression profiling experiment was performed in HeLa cells using an Affymetrix chip covering 47,000 transcripts and cRNA generated from cells irradiated in the presence of TO-RrRK or TO-FrFK. Differentially expressed genes were identified by comparing gene expression levels of irradiated to nonirradiated samples. TO-RrRK treatment followed by irradiation resulted in the identification of 66 mRNA probe sets with $\geq$2-fold change as compared to TO-RrRK treatment alone. Decreased gene expression occurred for 9 transcripts, whereas upregulation occurred for 57 transcripts. mRNAs represented by 52 probe sets changed $\geq$2-fold upon irradiation of TO-FrFK cells as compared to nonirradiated TO-FrFK cells. One transcript showed a decrease in gene expression, whereas 51 showed increased gene expression. The genes affected were primarily involved with transcriptional regulation, cell-cycle regulation, protein processing, nucleic-acid processing, carbohydrate processing, or apoptotic regulation—all cellular functions expected to be influenced by the production of ROS (Figure 3B).

In order to deconvolute the organelle-specific stress responses, we looked for genes from the microarray experiment that responded differently to mitochondrial or nuclear stress. We identified 22 genes with at least 2-fold higher expression corresponding specifically to nuclear oxidative stress, whereas 5 genes showed at least 2-fold higher expression levels with mitochondrial oxidative stress. Expression profiles of several genes demonstrating this type of differential response were verified using real-time PCR (Table 1).

Genes upregulated to a greater degree in response to nuclear stress than in response to mitochondrial stress included *atf3* and *v-jun*, two transcription factors known to be involved in the stress response [17, 18]. Analysis of the genes upregulated in response to mitochondrial stress yielded an intriguing finding: the expression of *areg* and *ereg*, genes encoding the growth factors Amphiregulin and Epiregulin, were significantly upregulated. Although Amphiregulin and Epiregulin were previously implicated in the stress response triggered by DNA-damaging agents and fine particulate matter [19–21], this is the first study, to our knowledge, to directly link these factors with mitochondrial stress. Both proteins are thought to play roles in apoptotic triggering, and could potentially buffer cells against the effects of low levels of endogenous oxidative stress. In addition, the expression levels of a third gene, early growth response 3 (*egr3*), were significantly higher for mitochondrial stress relative to nuclear stress. The protein encoded by *egr3* is a transcription factor, and is known to be involved in the control of Fas-mediated apoptosis [22].

A set of genes was also identified that responded similarly to mitochondrial and nuclear stress. *cox2*, *btg2*, and *gadd45b* transcript levels were all increased by >3-fold relative to controls. All three of these genes are influenced by the presence of oxidants [23, 24], and it appears that the subcellular origin of the ROS in HeLa cells is not an important factor in their upregulation.

The set of genes discussed above was also analyzed in MRC-5 cells (Table 2) to determine whether the subcellular response to oxidative stress is cell line specific. Four of the eight genes tested responded to mitochondrial and nuclear stress in the same manner in both cell lines: *areg*, *cox2*, *gadd45b*, and *atf3*. There were also distinct differences in gene expression between the two cell lines. In particular, *gadd45b* and *v-jun* were only upregulated with TO-RrRK in MRC-5 cells, whereas these genes were upregulated by both TO-RrRK and TO-FrFK in HeLa cells. *egr3* also had differential responses between the two cell lines, with higher upregulation in response to mitochondrial stress than nuclear stress in HeLa cells but not in MRC-5 cells. In addition, expression of the growth factor Epiregulin was increased in response to both mitochondrial and nuclear stress in MRC-5 cells, in

Table 2. Gene Expression Changes Measured by Real-Time PCR for Mitochondrial (TO-FrFK) and Nuclear (TO-RrRK) Oxidative Stress in MRC-5 Cells

Gene	Fold Change Relative to Control	
	TO-FrFK	TO-RrRK
TO-FrFK > TO-RrRK		
areg	4.4 (0.8)	2.7 (0.6)
TO-FrFK = TO-RrRK		
ereg	4.6 (0.5)	4.0 (0.5)
egr3	4.0 (0.8)	5 (1)
cox2	2.3 (0.7)	3.7 (0.5)
TO-FrFK < TO-RrRK		
btg2	2 (1)	4 (1)
gadd45b	0.9 (0.1)	4 (2)
atf3	48 (6)	73 (12)
jun	1.6 (0.4)	7 (1)

areg, amphiregulin; *ereg*, epiregulin; *egr3*, early growth response 3; *cox2*, cyclooxygenase-2; *btg2*, BTG family, member 2; *gadd45b*, growth arrest and DNA damage inducible, β; *atf3*, activating transcription factor 3; *jun*, v-jun avian sarcoma virus 17 oncogene. Numbers in parentheses represent standard deviation values.

contrast to it not being affected by nuclear stress in HeLa cells. Overall, the comparison of organelle-specific responses in the two cell lines indicated that there may be similar mechanisms underlying the differential levels of apoptosis seen in both cell lines. However, as described, we also uncovered variations in the genomic responses of these two cell lines which may reflect the inherent differences in cell type.

The studies outlined here demonstrate that synthetic peptide conjugates can be designed to access specific subcellular organelles and, with delivery of a photoactive oxidant, induce organelle-specific oxidative stress. Oxidative stress induces different levels of apoptosis and survival responses that depend upon the subcellular origin of the stress. Gene expression profiling suggests that different genes and levels of gene expression are involved in the response to mitochondrial and nuclear oxidative stress. The differences in survival responses and gene expression upon treatment with TO-FrFK and TO-RrRK may account for the differential cytotoxicities seen upon induction of site-specific oxidative damage. These studies indicate that the approach described will allow the identification of specific mechanisms that underlie the subcellular response to oxidative stress.

SIGNIFICANCE

The compounds described here represent a class of molecules that can be generated using chemical methods and used to elucidate new insights into oxidative stress pathways. In the studies described, the differential response mounted by cells subjected to mitochondrial or nuclear oxidative stress is deconvoluted and shown to differ significantly. It is noteworthy that a variety of elegant approaches based on the use of recombinant proteins are also available to generate ROS and other reactive species in living cells. Techniques such as chromophore-assisted light inactivation (CALI) [25, 26] and FLAsH (a technique relying on protein tags containing fluorescein arsenoxide conjugates) [27] can be used to direct oxidative or chemical stress at individual proteins or cellular structures. Using these methods, however, requires molecular biology expertise, careful transfection analysis, and cell sorting to isolate a population of cells suitable for study. The reagents described here represent an alternative to protein-based agents and may be more amenable to chemical manipulation.

In addition to providing important information about the oxidative stress response that is initiated by ROS originating in different organelles, the finding that nuclear and mitochondrial oxidative stress exert different levels of cell death and a different cellular response has important implications for the development of improved agents for photodynamic therapy (PDT). PDT relies on photoactive compounds like those described here that cause cell death via photoinitiated ROS production [28, 29]. The observation that nuclear localization of ROS produces higher levels of toxicity indicates that the potency of PDT therapies could be increased if therapeutic compounds were directed to this organelle.

We have demonstrated that by engineering compounds that localize differentially within human cells, the oxidative stress response can be studied and separated into discrete components. This approach presents a powerful means to systematically investigate cellular function with increased precision, and demonstrates that stress originating in different organelles is linked to unique responses.

EXPERIMENTAL PROCEDURES

Detailed descriptions of all experimental procedures and characterization of representative compounds are provided in the Supplemental Data.

Preparation of TO-Peptide Conjugates

TO-peptide conjugates were prepared as described previously [10]. See the Supplemental Data for protocols and characterization information.

Cell Culture

HeLa 229 cells (ATCC) or MRC-5 cells (ATCC) were cultured as subconfluent monolayers on 25 cm^2 or 75 cm^2 cell-culture plates with vent caps in 1× minimum essential α medium (MEM; GIBCO) supplemented with fetal bovine serum (10% v/v; ATCC) in a humidified incubator at 37°C containing CO_2 (5%). HeLa cells were derived from a cervical cancer epithelial cell line; the MRC-5 cells were a transformed lung fibroblast cell line.

Characterization of Localization Profiles for TO Conjugates

HeLa cells that had been grown to subconfluence were dissociated from the surface with a solution of 0.05% trypsin/0.53 mM EDTA for 10 min at 37°C. Aliquots of 1×10^5 cells were plated in four-well borosilicate glass-bottom coverslips and cultured overnight to allow cell adherence. The culture medium was removed, and the cells were rinsed in 1× Ca^{2+}- and Mg^{2+}-free phosphate-buffered saline. HeLa cells were incubated for 90 min at 37°C under 5% CO_2/humidity with serum-free MEM containing 5 μM peptide conjugate. Images were taken with an inverted Leica TCS SP2 scanning confocal microscope with an oil immersion lens (63×). The excitation wavelength for visualization of TO conjugates ($\lambda_{ex\ max}$ = 501 nm) was 488 nm, and emission was collected from 500 to 550 nm. The illumination conditions were optimized such that cell viability and integrity were maintained. A large number of independent trials (>20) were performed to verify that the localization trends reported were accurate. See the Supplemental Data for protocols used in colocalization experiments.

Cell-Counting Kit 8 Cytotoxicity Assay

HeLa or MRC-5 cells were grown to subconfluence and harvested into Liebovitz's L-15 medium containing 10% fetal bovine serum. Cells were seeded at a concentration of 10,000 cells/well in a 96-well plate (Nunc) and allowed to adhere overnight at 37°C. TO-conjugate solution was added to yield a concentration of 5 μM in complete L-15 (without phenol red), and the plate was incubated for 90 min at 37°C. The plate was irradiated using a Lumacare noncoherent light source equipped with a custom fiber optic probe (500 ± 25 nm range) for 0–30 min. Following irradiation, the media were removed and replaced with complete L-15. The plate was incubated for 13 hr at 37°C. The media were then replaced with 10% (v/v) CCK-8 dye (Dojindo) in complete L-15 (100 μl total volume) and incubated for 2 hr. The $OD_{450\ nm}$ of each sample was determined using a Spectramax M5 microplate reader (Molecular Devices).

Flow Cytometry and Confocal Analysis of Annexin V Binding

HeLa cells were trypsinized and harvested with complete L-15 as described above. Cells were seeded at 30,000 cells/well in a 24-well plate (Nunc) and allowed to adhere overnight at 37°C. The media were removed and replaced with complete L-15 containing 5 μM appropriate TO conjugate and incubated for 90 min at 37°C. Wells were then individually irradiated for 20 min using an Oriel light source equipped with a fiber optic probe (500 ± 10 nm). Following irradiation, the media were removed and replaced with complete L-15 and incubated for 13 hr at 37°C. Following overnight incubation, the cells were washed, treated with trypsin/EDTA, and pelleted. Following an additional PBS wash, the cells were resuspended in binding buffer containing 5 μl of Cy5-conjugated Annexin V (BD Biosciences) and 5 μl of propidium iodide (PI; 50 μg/ml; BD Biosciences). The samples were analyzed by flow cytometry on a BD FACSCanto flow cytometer (BD Biosciences) using FACSDiva software (BD Biosciences). See the Supplemental Data for further details and description of experiments where zVAD or survival pathway inhibitors were employed. Experiments for confocal microscopy were prepared in a similar manner. See the Supplemental Data for details.

Preparation of Samples for Microarray Analysis

HeLa cells were seeded in separate 12-well plates at 400,000 cells/well in complete L-15 media and allowed to adhere to the surface overnight at 37°C. Solutions (5 μM) of the appropriate TO conjugate were then added in complete L-15 and incubated for 90 min at 37°C. After incubation, the samples were irradiated at 500 ± 10 nm for 25 min using an Oriel light source. Following irradiation, the media containing conjugate were removed and replaced with complete L-15 and incubated for 2 hr at 37°C. Cells were then harvested and total RNA was isolated using a QIAGEN RNeasy kit with on-column DNase treatment. The samples were processed at the Boston University Microarray Facility to obtain biotinylated cRNA samples.

Microarray analysis was performed using the Affymetrix U133 2.0 Plus Human GeneChip. TO-FrFK and TO-RrRK nonirradiated samples were analyzed in duplicate, whereas irradiated samples were analyzed in triplicate. A two-way ANOVA identified 326 genes with differential expression among the four samples. All transcripts had P values $\leq$ 0.001, giving a false discovery rate of 10%. All 326 genes were considered "present" by GeneChip software, and showed similar expression levels among replicates. Genes showing $\geq$2-fold change in expression levels as compared to control cells (74 genes total) were considered significant.

Real-Time PCR

The gene expression of irradiated and nonirradiated TO-FrFK, TO-RrRK, and untreated HeLa or MRC-5 cell samples were determined for eight different primer sets corresponding to genes identified by microarray analysis. HeLa cells were treated as described above, and total RNA was isolated. Reverse transcription using oligo d(T)18 primers was performed using a Retroscript kit (Ambion). SybrGreen-based qRT-PCR was performed on a Bio-Rad iCycler using gene-specific primers (Table S1). Real-time PCR was performed on MRC-5 cells in an analogous manner.

Supplemental Data

Supplemental Data include five figures, two tables, experimental and synthetic protocols, and a list of genes from microarray experiments and are available at http://www.chembiol.com/cgi/content/full/14/8/923/DC1/.

ACKNOWLEDGMENTS

We thank the NSF (CAREER award to S.O.K.), the Sloan Foundation, and the Dreyfus Foundation for their support of this work. We also acknowledge James Jonkman and the Advanced Optical Microscopy Facility at Princess Margaret Hospital for expert assistance with confocal fluorescence imaging.

Received: May 23, 2007
Revised: July 3, 2007
Accepted: July 5, 2007
Published: August 24, 2007

REFERENCES

1. Finkel, T., and Holbrook, N. (2000). Oxidants, oxidative stress and the biology of ageing. Nature *408*, 239–247.
2. Giasson, B.I., Duda, J.E., Murray, I.V., Chen, Q., Souza, J.M., Hurtig, H.I., Ischiropoulos, H., Trojanowski, J.Q., and Lee, V.M. (2000). Oxidative damage linked to neurodegeneration by selective α-synuclein nitration in synucleinopathy lesions. Science *290*, 985–989.
3. Chuang, Y.Y., Chen, Y., Gadisetti, C., Cook, J.A., Coffin, D., Tsai, M.H., DeGraff, W., Yan, H., Zhao, S., Russo, A., et al. (2002). Gene expression after treatment with hydrogen peroxide, menadione, or t-butyl hydroperoxide in breast cancer cells. Cancer Res. *62*, 6246–6254.
4. Croteau, D.L., and Bohr, V.A. (1997). Repair of oxidative damage to nuclear and mitochondrial DNA in mammalian cells. J. Biol. Chem. *272*, 25409–25412.
5. Murray, J.I., Whitfield, M.L., Trinklein, N.D., Myers, R.M., Brown, P.O., and Botstein, D. (2004). Diverse and specific gene expression responses to stresses in cultured human cells. Mol. Biol. Cell *15*, 2361–2374.
6. Martindale, J.L., and Holbrook, N.J. (2002). Cellular response to oxidative stress: signaling for suicide and survival. J. Cell. Physiol. *192*, 1–15.
7. Harris, S.L., and Levine, A.J. (2005). The p53 pathway: positive and negative feedback loops. Oncogene *24*, 2899–2908.

8. Hansen, J.M., Go, Y.M., and Jones, D.P. (2006). Nuclear and mitochondrial compartmentation of oxidative stress and redox signaling. Annu. Rev. Pharmacol. Toxicol. *46*, 215–234.
9. Mahon, K.P., Jr., Ortiz-Meoz, R.F., Prestwich, E.G., and Kelley, S.O. (2003). Photosensitized DNA cleavage promoted by amino acids. Chem. Commun. *15*, 1956–1957.
10. Carreon, J.R., Mahon, K.P., Jr., and Kelley, S.O. (2004). Thiazole orange-peptide conjugates: sensitivity of DNA binding to chemical structure. Org. Lett. *6*, 517–519.
11. Silva, G.L., Ediz, V., Yaron, D., and Armitage, B.A. (2007). Experimental and computational investigation of unsymmetrical cyanine dyes: understanding torsionally responsive fluorogenic dyes. J. Am. Chem. Soc. *129*, 5710–5718.
12. Ross, M.F., Filipovska, A., Smith, R.A., Gait, M.J., and Murphy, M.P. (2004). Cell-penetrating peptides do not cross mitochondrial membranes even when conjugated to a lipophilic cation: evidence against direct passage through phospholipid bilayers. Biochem. J. *383*, 457–468.
13. Wender, P.A., Mitchell, D.J., Pattabiraman, K., Pelkey, E.T., Steinman, L., and Rothbard, J.B. (2000). The design, synthesis, and evaluation of molecules that enable or enhance cellular uptake: peptoid molecular transporters. Proc. Natl. Acad. Sci. USA *97*, 13003–13008.
14. Tamaoki, T., Nomoto, H., Takahashi, I., Kato, Y., Morimoto, M., and Tomita, F. (1986). Staurosporine, a potent inhibitor of phospholipid/Ca^{++}dependent protein kinase. Biochem. Biophys. Res. Commun. *135*, 397–402.
15. Dudley, D.T., Pang, L., Decker, S.J., Bridges, A.J., and Saltiel, A.R. (1995). A synthetic inhibitor of the mitogen-activated protein kinase cascade. Proc. Natl. Acad. Sci. USA *92*, 7686–7689.
16. Vlahos, C.J., Matter, W.F., Hui, K.Y., and Brown, R.F. (1994). A specific inhibitor of phosphatidylinositol 3-kinase, 2-(4-morpholinyl)-8-phenyl-4H-1-benzopyran-4-one (LY294002). J. Biol. Chem. *269*, 5241–5248.
17. Hai, T., and Hartman, M.G. (2001). The molecular biology and nomenclature of the activating transcription factor/cAMP responsive element binding family of transcription factors: activating transcription factor proteins and homeostasis. Gene *273*, 1–11.
18. Shaulian, E., and Karin, M. (2002). AP-1 as a regulator of cell life and death. Nat. Cell Biol. *4*, E131–E136.
19. Berasain, C., Garcia-Trevijano, E.R., Castillo, J., Erroba, E., Santamaria, M., Lee, D.C., Prieto, J., and Avila, M.A. (2005). Novel role for amphiregulin in protection from liver injury. J. Biol. Chem. *280*, 19012–19020.
20. Blanchet, S., Ramgolam, K., Baulig, A., Marano, F., and Baeza-Squiban, A. (2004). Fine particulate matter induces amphiregulin secretion by bronchial epithelial cells. Am. J. Respir. Cell Mol. Biol. *30*, 421–427.
21. Miyazaki, Y., Shinomura, Y., Tsutsui, S., Yasunaga, Y., Zushi, S., Higashiyama, S., Taniguchi, N., and Matsuzawa, Y. (1996). Oxidative stress increases gene expression of heparin-binding EGF-like growth factor and amphiregulin in cultured rat gastric epithelial cells. Biochem. Biophys. Res. Commun. *226*, 542–546.
22. Droin, N.M., Pinkoski, M.J., Dejardin, E., and Green, D.R. (2003). Egr family members regulate nonlymphoid expression of Fas ligand, TRAIL, and tumor necrosis factor during immune responses. Mol. Cell. Biol. *23*, 7638–7647.
23. Choi, E.M., Heo, J.I., Oh, J.Y., Kim, Y.M., Ha, K.S., Kim, J.I., and Han, J.A. (2005). COX-2 regulates p53 activity and inhibits DNA damage-induced apoptosis. Biochem. Biophys. Res. Commun. *328*, 1107–1112.
24. Rouault, J.P., Falette, N., Guehenneux, F., Guillot, C., Rimokh, R., Wang, Q., Berthet, C., Moyret-Lalle, C., Savatier, P., Pain, B., et al. (1996). Identification of BTG2, an antiproliferative p53-dependent component of the DNA damage cellular response pathway. Nat. Genet. *14*, 482–486.
25. Tour, O., Meijer, R.M., Zacharias, D.A., Adams, S.R., and Tsien, R.Y. (2003). Genetically targeted chromophore-assisted light inactivation. Nat. Biotechnol. *21*, 1505–1508.
26. Bulina, M.E., Chudakov, D.M., Britanova, O.V., Yanushevich, Y.G., Staroverov, D.B., Chepurnykh, T.V., Merzlyak, E.M., Shkrob, M.A., Lukyanov, S., and Lukyanov, K.A. (2006). A genetically encoded photosensitizer. Nat. Biotechnol. *24*, 95–99.
27. Remington, S.J. (2006). Fluorescent proteins: maturation, photochemistry and photophysics. Curr. Opin. Struct. Biol. *16*, 714–721.
28. Dolmans, D.E., Fukumura, D., and Jain, R.K. (2003). Photodynamic therapy for cancer. Nat. Rev. Cancer *3*, 380–387.
29. Brown, S.B., Brown, E.A., and Walker, I. (2004). The present and future role of photodynamic therapy in cancer treatment. Lancet Oncol. *5*, 497–508.

